Ceramics International 50 (2024) 7767–7774

Contents lists available at ScienceDirect

Ceramics International

journal homepage: www.elsevier.com/locate/ceramint

$Ca_3ZnAl_4O_{10}$: A novel Al-rich microwave dielectric ceramic with low-ε_r

Congxue Su [a,*], Junhao Zheng [a], Pengxiang Gao [b], Xingliu Qin [a], Kuo Liu [a], Fengqi Lu [b], Junqi Chen [d,**], Laiyuan Ao [e], Huanfu Zhou [b,***]

[a] Guangxi Key Lab of Agricultural Resources Chemistry and Biotechnology, College of Chemistry and Food Science, Yulin Normal University, Yulin, 537000, China
[b] Collaborative Innovation Centre for Exploration of Hidden Nonferrous Metal Deposits and Development of New Materials in Guangxi, Key Laboratory of Nonferrous Materials and New Processing Technology, Ministry of Education, School of Materials Science and Engineering, Guilin University of Technology, Guilin, 541004, China
[d] School of Mechanical Engineering, Guilin University of Aerospace Technology, Guilin, 443002, China
[e] China Zhenhua Group Yunke Electronic Co. Ltd., Guiyang, 550018, China

ARTICLE INFO

Handling Editor: P. Vincenzini

Keywords:
Microwave dielectric properties
$Ca_3ZnAl_4O_{10}$
Bond valence
Rattling effect

ABSTRACT

Low-ε_r microwave dielectric ceramics $Ca_3ZnAl_4O_{10}$ with orthorhombic structure were fabricated by solid-state reaction process. Good grain uniformity and compact microstructure were observed at 1290 °C. Single phase $Ca_3ZnAl_4O_{10}$ ceramics were obtained at the range of 1250–1330 °C and exhibited promising microwave dielectric properties with ε_r = 8.11–8.31, $Q\times f$ = 23,060–30,750 GHz and τ_f = −27.5 to −23.3 ppm/°C. The larger positive deviations between ε_{theo} and ε_{corr} as well as the smaller $|\tau_f|$value could be ascribed to the strong "rattling" effect. The calculated bond valence show that Ca^{2+}, Al^{3+} are "rattling" cations while Zn^{2+} is "compressed" cation. Furthermore, the $Q\times f$ values is mainly affected by the density and packing fraction.

1. Introduction

The rapid development of wireless communication technology has facilitated the widespread application of microwave dielectric ceramics as key materials for substrates, resonators, filters and other devices. Due to low latency, large capacity and high transfer rate are the major characteristics of 5G technology, microwave dielectric materials with acceptable permittivity (ε_r) and high quality factor ($Q\times f$) have received extensive attention [1–3]. Low latency is one of the key enablers of 5G technology to serve multiple emerging applications having diverse requirements. To accomplish the faster signal transmission speed and shorten the signal delay time (t_d), dielectrics with a low permittivity ($\varepsilon_r < 10$) have become a research hotpot since t_d is proportional to $\sqrt{\varepsilon_r}$ [4,5].

There have been various low-ε_r ceramics systems reported in the last decade including borates, aluminates, silicates, germanates, vanadates, phosphates, and molybdates [6–12]. Compared to the other systems, borates, vanadates and phosphates usually have a significant advantage in low sintering temperature but suffer from the drawbacks of moisture absorption and the porous microstructures caused by the volatilisation of low melting point components. Germanates have a moderate sintering temperature, but are not suitable for mass production by reason of expensive GeO_2. Aluminates and silicates have been widely welcomed because of their low-cost raw materials, easy fabrication, material stability, and non-absorbent. Moreover, the feature of low permittivity in Al-based systems comes mainly from the low ionic polarizability of Al^{3+} (0.79 $Å^3$) and the strong covalent bonds in different kinds of [Al-O] polyhedrons. Consequently, aluminates have garnered considerable attention [13–23]. For example, Lan et al. [13] have reported that $LiAl_5O_8$ with an inverse-spinel structure sintered at 1600 °C possessed the properties of ε_r = 8.43, $Q\times f$ = 49,300 GHz, and τ_f = −38 ppm/°C. Spinels with the general formula of $M^{2+}Al_2O_4$ have lower sintering temperature (1425–1460 °C) and higher $Q\times f$ value compared with the $LiAl_5O_8$ ceramic, such as $MgAl_2O_4$ (ε_r = 8.2, $Q\times f$ = 68,900 GHz, τ_f = −75 ppm/°C) [19] and $ZnAl_2O_4$ (ε_r = 8.5, $Q\times f$ = 56,300 GHz, τ_f = −79 ppm/°C) [22]. Liu et al. reported $CaAl_2O_4$ ceramic sintered at 1450 °C exhibited superior properties of ε_r = 8.9, $Q\times f$ = 91,350 GHz, and τ_f = −55 ppm/°C [20]. Besides, other Al-rich ceramics in grossite-type [14], melilite-type [15], ramsayite-type [16], sillimanite-type [17], and hexacelsian-type [18] also have desirable microwave dielectric properties (Table 1).

As another Al-rich compound, $Ca_3ZnAl_4O_{10}$ was first synthesized at

* Corresponding author.
** Corresponding author.
*** Corresponding author.
E-mail addresses: alpes1987@163.com (C. Su), junqichen1991@163.com (J. Chen), zhouhuanfu@163.com (H. Zhou).

https://doi.org/10.1016/j.ceramint.2023.12.103
Received 23 August 2023; Received in revised form 21 October 2023; Accepted 8 December 2023
Available online 12 December 2023

Table 1
Microwave dielectric properties of some Al-based ceramics with $\varepsilon_r < 10$.

Ceramics	ST (°C)	ε_r	$Q\times f$ (GHz)	τ_f (ppm/°C)	Ref
$LiAl_5O_8$	1600	8.43	51,700	−38	13
$CaAl_4O_7$	1575	8.45	25,500	−98	14
$Sr_2SiAl_2O_7$	1525	7.2	33,000	−37	15
$Ca_2Sn_{1.9}Zr_{0.1}Al_2O_9$	1525	8.67	77,800	−69.8	16
Al_2SiO_5	1525	4.4	41,800	−17	17
$BaAl_2Si_2O_8$	1475	6.36	44,800	−46.9	18
$MgAl_2O_4$	1460	8.75	68,900	−75	19
$CaAl_2O_4$	1450	8.9	91,350	−55	20
$Ca_2Sn_{1.92}Al_2O_{8.84}$	1450	8.3	105,700	−63.7	21
$ZnAl_2O_4$	1425	8.5	56,300	−79	22
$LiZn_{0.01}Si_{0.01}Al_{0.98}O_2$	1300	6.12	56,986	−122	23
$Ca_3ZnAl_4O_{10}$	1290	8.31	30,750	−23.3	This work

the temperature 1300–1350 °C by Barbanyagre et al. in 1997 [24], and subsequent investigations have focused on the host material for the production of reddish and bluish-emitting phosphors [25,26]. However, the microwave dielectric properties of $Ca_3ZnAl_4O_{10}$ ceramics have not been reported yet. In this work, $Ca_3ZnAl_4O_{10}$ ceramics were synthesized using the solid-state sintering reaction in the CaO–Al_2O_3–ZnO system. The crystal structure, sintering characteristics, microstructure, and microwave dielectric properties were discussed in detail.

2. Experimental procedure

High-purity powders of $CaCO_3$ (99.99 %, Aladdin), ZnO (99.99 %, Aladdin), and Al_2O_3 (99.99 %, Aladdin) were weighted according to $Ca_3ZnAl_4O_{10}$. The stoichiometric powders were ball-milled with alcohol at a speed of 250 r/min for 6 h. The slurries obtained were dried and calcined at 1180 °C for a 4 h solid-state reaction, and then reball-milled in alcohol for another 6 h. The acquired slurries were dried and compressed into cylindrical pellets ($\Phi = 10$ mm, $H = 6.5$ mm) mixed with 5 wt% polyvinyl alcohol (PVA). Next, above columnar samples were heated at 500 °C with a rate of 2 °C/min for 2 h to remove PVA. Finally, to limit Zn evaporation, the specimens were muffled in the powder of the same composition and sintered at 1250–1330 °C for 6 h.

The composition and phase structure of the sintered $Ca_3ZnAl_4O_{10}$ ceramics were investigated by X-ray powder diffraction using Panalytical X'pert Pro diffractometer with Cu Kα radiation in the 2θ range of 5–80°. The XRD data was refined according to Rietveld method by Fullprof software. Bulk densities of ceramics were measured through Archimedes method. Microstructure morphology in the ceramic samples was examined using Hitachi S4800 scanning electron microscope. The ε_r and $Q\times f$ values were measured by a network analyzer (Model E5071C, Agilent Co., CA). The τ_f value was obtained using the following equation:

$$\tau_f = \frac{f_{85} - f_{25}}{(85-25)\times f_{25}} \times 10^6 \quad (1)$$

where, f_{85} and f_{25} are the resonant frequencies at 85 °C and 25 °C, respectively.

3. Results and discussion

Fig. 1 compares the XRD profiles of the $Ca_3ZnAl_4O_{10}$ ceramics sintered at 1250–1330 °C for 6 h to the standard data (JCPDS 01-087-0266). By a comparison between them, no apparent additional crystal phase or diffraction peaks were generated in the ceramics. All peaks can be well indexed to a $Ca_3ZnAl_4O_{10}$ single phase crystallized in the space group *Pbc21*, indicating that the desired pure phase samples with orthorhombic structure were obtained successfully. To understand the crystal structure information in detail, Rietveld refinement was done using FullProf software. The Rietveld refinement pattern of the $Ca_3ZnAl_4O_{10}$ specimens at various temperatures are shown in Fig. 2(a–e), and

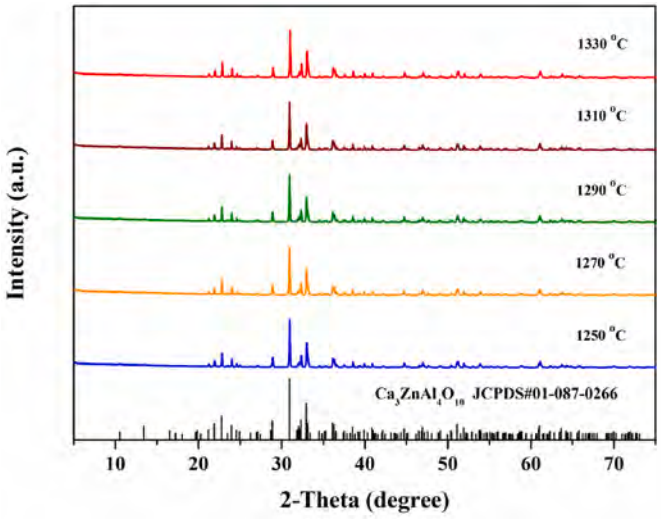

Fig. 1. X-Ray diffraction patterns of $Ca_3ZnAl_4O_{10}$ ceramics sintered at various temperatures ranging from 1250 °C to 1330 °C for 6 h.

the low refined reliability factors R_p, R_{wp}, and χ^2 are listed in Table 2. All the values of refinement parameters are less than 10 %, indicating that the calculated results are reliable. A schematic structure of $Ca_3ZnAl_4O_{10}$ is sketched in Fig. 2 (f). In the structure, a three-dimensional network are consisted of [ZnO_4] and [AlO_4] tetrahedrons in which Zn1 (8e Wyckoff position) and Zn2 (4d Wyckoff position) locate in the former tetrahedra while four kinds of Al cations locate in the latter tetrahedra. In the [AlO_4] tetrahedrons, Al1 and Al4 cations occupy the 8e and 4c Wyckoff position, while Al2 and Al3 cations occupy the 4d Wyckoff position respectively. All tetrahedra are linked each other only by corner-sharing and connect the [CaO_6] octahedrons in the form of edge-sharing or angle-sharing. There two kinds of Wyckoff positions of Ca^{2+} in the octahedron. The Ca1 and Ca3 cations at 8e Wyckoff position are symmetrically located in two edge-sharing octahedrons. Ca2 cations in the 4d Wyckoff position are located in the [Ca2O_6] octahedrons, and these octahedrons share edge with [Ca1O_6] and [Ca3O_6] octahedrons. A channel is composed of six tetrahedrons with center calcium atoms Ca2, which are surrounded by eight nearest neighbors O anions with 4d and 8e Wyckoff positions (as shown in the red short-dashed circle). Ca1 (Ca3) cations are surrounded by six nearest oxygen neighbors (O1 and O2 at 4d, O4, O6 and O7 at 8e, and O5 at 4b Wyckoff site) and it can be seen from the blue short-dashed circle. Accordingly, these coordination environment can be represented as distorted [CaO_6] octahedra and [CaO_8] square antiprism, respectively [27].

Figs. 3 and 4 present the typical SEM images of $Ca_3ZnAl_4O_{10}$ ceramics sintered at 1250–1330 °C and their corresponding grain size distributions. For the ceramic sintered at 1250 °C, the surface morphology of sample displayed relatively compact and the small grains below 1.5 μm were preponderant inside the ceramic. The average grain size increased slightly to 1.69 μm and dense microstructure with clear grain boundaries were developed at 1270 °C. Further sintering to 1290 °C, the surface morphology of ceramic changed to denser and more uniform, following the increase in particle size. The grain uniformity in microstructure could be confirmed by Fig. 4 (c), which reveals the grain size distribution is mainly within the range 0.8–2.4 μm. When the ceramic was sintered at 1310 °C, the phenomenon of abnormal grain growth appeared, and the average grain size increased to 2.73 μm rapidly. Meanwhile, some grains began to melt and the grain boundaries became blurred, all indicating that over-sintering had occurred. With increasing the sintering temperature to 1330 °C, the liquid-like areas occurred. Many small grains were trapped within or between the abnormally grown large grains, perhaps by reason of some abnormal grain benefited from the liquid phase would suppress the grain growth of

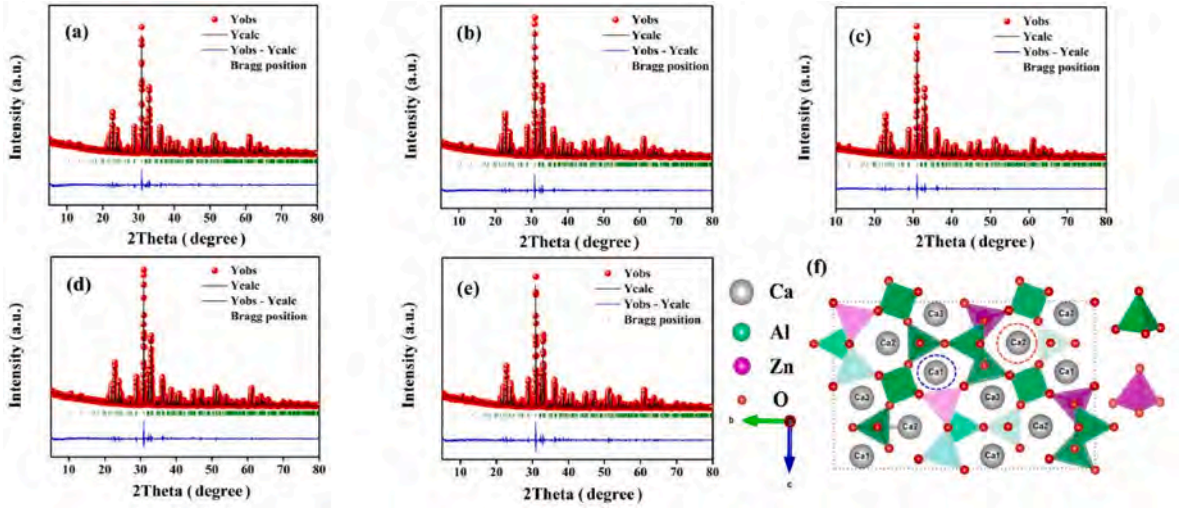

Fig. 2. Rietveld XRD patterns of $Ca_3ZnAl_4O_{10}$ ceramics sintered at various temperatures for 6 h (a) 1250 °C, (b) 1270 °C, (c) 1290 °C, (d) 1310 °C, (e) 1330 °C, and (f) is the schematic diagram of $Ca_3ZnAl_4O_{10}$ structure.

Table 2
Refinement parameters and reliability of $Ca_3ZnAl_4O_{10}$ ceramics.

Structural parameters	S.T. (°C)				
	1250	1270	1290	1310	1330
a (Å)	5.1389 (2)	5.1387 (2)	5.1384 (2)	5.1386 (2)	5.1392 (2)
b (Å)	16.7394 (3)	16.7386 (3)	16.7379 (2)	16.7430 (3)	16.7441 (3)
c (Å)	10.7188 (2)	10.7183 (2)	10.7184 (3)	10.7167 (3)	10.7173 (3)
$\alpha = \beta = \gamma$ (°)	90	90	90	90	90
V (Å^3)	922.05 (2)	921.93 (2)	921.85 (2)	922.02 (3)	922.24 (3)
R_p (%)	6.79	6.60	6.61	7.07	7.31
R_{wp} (%)	8.92	8.67	8.62	9.31	9.55
χ^2	1.33	1.24	1.24	1.42	1.49

other grains [28]. The coexistence of exaggerated large and small particles, which could be seen from the grain size distributions in Fig. 4 (e), leading to the degradation in grain uniformity.

To provide a further insight into the uniformity of grain distribution, the grain size distribution of samples was statistically analyzed by Origin, as shown in Table S1. Then, Gaussian fitting was performed base on the statistical results (as shown in Fig. 4 and Table S1). The grain size distribution was in accord with the normal distribution (Adjusted R-squared >0.85) and the standard deviation was small as sintering temperature rose from 1250 °C to 1290 °C. These results showed that the grain size distribution was uniform, which was the phenomenon of normal grain growth. Abnormal grain growth occurred at 1310 °C, and the grain size distribution had deviated from the normal distribution with the relative high standard deviation of 1.7985. As the sintering temperature was further increased to 1330 °C, the grain size distribution of the ceramic did not obey a normal distribution (Adjusted R-squared <0.5), and the high standard deviation of 3.6797 indicated that the grain size distribution in this sample was very irregular. This similar phenomenon could be also found in the $KSrPO_4$ [29] and $La_5Sn_4O_{15}$ ceramics [30].

Fig. 5 depicts the bulk density, relative density, relative permittivity, and pore-corrected permittivity of $Ca_3ZnAl_4O_{10}$ ceramics as functions of sintering temperature. As illustrated in Fig. 5 (a), the bulk density and relative density of $Ca_3ZnAl_4O_{10}$ ceramics raise first and then decline with the rise of sintering temperature, which is in accordance with the microstructure evolution. From 1250 °C to 1290 °C, the bulk density increases monotonously from 96.23 % of the theoretical density (3.267 g/cm^3) to 96.93 % of the theoretical density (3.268 g/cm^3). Further increasing the sintering temperature results in a decline of relative density to 95.65 % at 1330 °C, giving an optimum sintering temperature of $Ca_3ZnAl_4O_{10}$ to be 1290 °C. The improvement and decline in density are due to the grain growth and over-sintering, respectively, which is consistent with the SEM characterization.

As shown in Fig. 5 (b), increasing sintering temperature brings about an increase of the relative permittivity ε_r, which reaches a maximum value of 8.36 at 1290 °C. A downward trend of ε_r is observed with the further increase in the sintering temperature, which is kept in step by the trend of density. Considering that the relatively small permittivity of air (about 1) trapped in the pores would also affect the ε_r, the pore-corrected permittivity (ε_{corr}) was calculated to exclude the influence of porosity on ε_r through Bosman and Havinga's correction [31]:

$$\varepsilon_{corr} = \varepsilon_r (1 + 1.5p) \quad (2)$$

where P is the fractional porosity. Different sintering temperatures resulted in limited variation in the calculated ε_{corr} values, and these ε_{corr} values were a little higher than the ε_r values with a minimal deviation of 4.6 % between them. The total polarizability (α) and the molar volume (V_m) significantly affect the ε_r in the microwave frequency region. Therefore, the theoretical permittivity ε_{theo} of $Ca_3ZnAl_4O_{10}$ ceramics can be calculated by the Clausius–Mossotti (C-M) equation and additive rule [32,33]:

$$\varepsilon_{theo} = \frac{3V_m + 8\pi\alpha}{3V_m - 4\pi\alpha} \quad (3)$$

$$\alpha_{\text{theo}} = 3\alpha(Ca^{2+}) + \alpha(Zn^{2+}) + 4\alpha(Al^{3+}) + 10\alpha(O^{2-}) \quad (4)$$

where α_{theo} and V_m are the sum polarizability and molar volume, respectively.

As shown in Table 3, the ε_{theo} values of $Ca_3ZnAl_4O_{10}$ ceramics vary from 6.150 to 6.155, which are obviously lower than their ε_{corr} values with positive deviations [$\Delta\varepsilon_r = (\varepsilon_{corr} - \varepsilon_{theo})/\varepsilon_{theo}$] of 39.45–41.23 %. Shannon ascribed the large deviations ($\Delta\varepsilon_r$ = 13–44 %) in ε_{corr} and ε_{theo} to the presence of "rattling" cations [33]. The rattling effect was described by Dunitz and Orgel as follow, when the central cation at the polyhedron becoming loosening, the polyhedron would change its configuration to adapt the cation, thereby resulting in a polyhedral distortion and corresponding to the higher polarizability [34]. Similar phenomenon occurred in $Mg_xY_{3-x}Al_{5-x}Si_xO_{12}$ (x = 0.1–0.6) [35] and $REVO_4$ (RE = Yb, Ho) [36] due to the rattling effect of the cation sites, which can be understood by bond valence (BV, V_i) [37,38]:

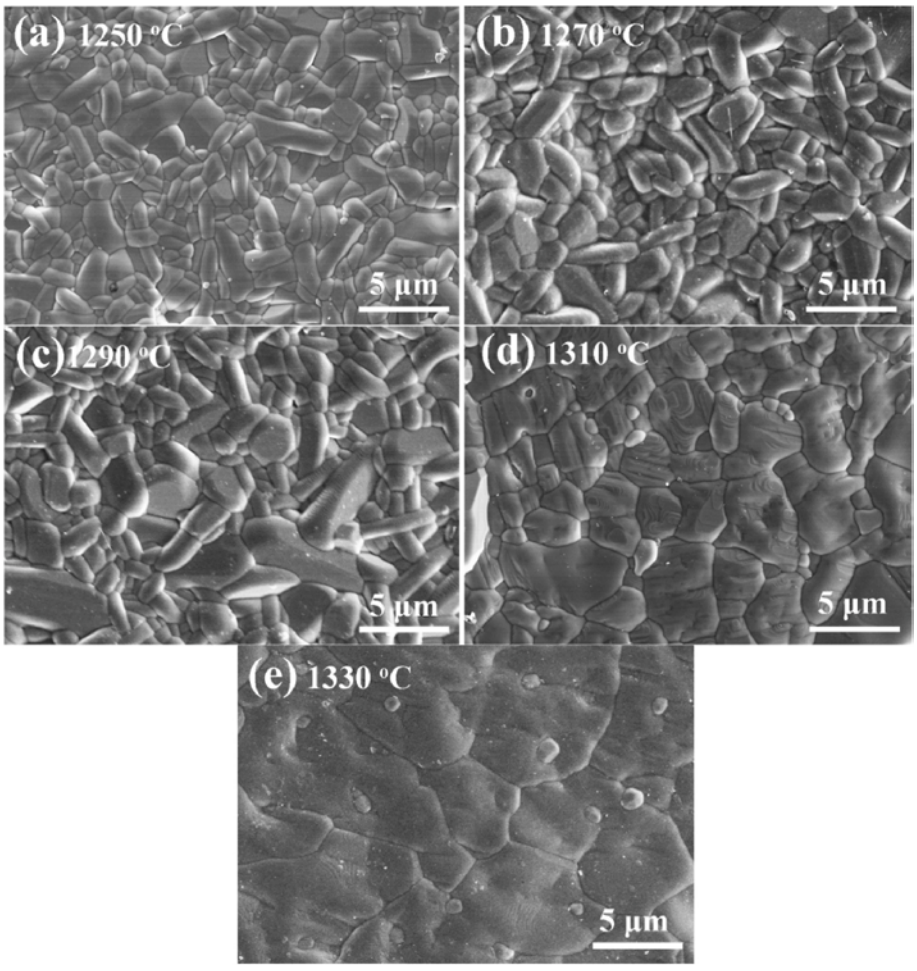

Fig. 3. SEM images of the $Ca_3ZnAl_4O_{10}$ ceramics sintered at different temperatures for 6 h (a) 1250 °C, (b) 1270 °C, (c) 1290 °C, (d) 1310 °C, (e) 1330 °C.

$$v_{ij} = exp\left[\frac{R_{ij} - d_{ij}}{b}\right] \tag{5}$$

$$V_{ij} = \sum v_{ij} \tag{6}$$

where R_{ij} is the bond valence parameter, d_{ij} is the bond length between atom i and j measured by the Rietveld refinement results, and b is the constant 0.37 Å. The bond valence of each ion in $Ca_3ZnAl_4O_{10}$ sintered at 1290 °C are listed in Table 4. The bond valance of Ca^{2+} are less than the ideal valence of 2 v.u., especially the Ca^{2+} adopted eight-coordinated exhibits a smaller value of 1.5607 v.u., suggesting that this Ca^{2+} to be the "rattling" cation in its polyhedron. Likewise, all the Al^{3+} show smaller bond valences than their normal valence of 3 v.u., suggesting these "rattling" cation Al^{3+} are small for the tetrahedral site. As for Zn^{2+}, the bond valence (3.0115 v.u.) is bigger than its ideal valence of 2 v.u., showing "compressed" cation Zn is tightly bound in the tetrahedra. Therefore, the large $\Delta\varepsilon_r$ might be ascribed to the strong rattling effect caused by Ca^{2+} and Al^{3+} in their distorted polyhedra.

To our knowledge, the τ_f of most microwave ceramics with low-ε_r is mainly affected by the structural factors, in which bond valence is an important factor to understand the structure-activity relationship [39]. For the orthorhombic structured $Ca_3ZnAl_4O_{10}$ with a complex framework, the bond valence of eight-, six- and four-coordinated site cations should be considered. Then the relationship between τ_f value and the sum of cation bond valence is illustrated in Fig. 6 (a) and Table 5. The lower bond valence means the weaker bond strength in the polyhedra, which leads to a smaller restoring force to recover the deformation of the polyhedra, thereupon a shift of τ_f value in the positive direction happens [40]. Viewed from another perspective, τ_f can be explained by the temperature coefficient of dielectric constant (τ_ε) and the coefficient of the thermal expansion (α_L) through relationship $\tau_f = -(\alpha_L + 0.5\tau_\varepsilon)$. For $Ca_3ZnAl_4O_{10}$ ceramic sintered at its optimum temperature, the τ_ε value measured at microwave frequency between 25 °C and 85 °C is 35.4 ppm/°C. The α_L value calculated from the relationship mention above is 5.6 ppm/°C, thus τ_f is mainly driven by τ_ε since the value of latter is bigger than that of α_L. The differential equation (Eq. 7) derived from C-M equation by Bosman and Havingais [31] in favor of understanding τ_ε from the structural point of view. This equation describes the relationship among τ_ε ε_r, α_L, and the temperature coefficient of ionic polarizability ($\tau_{\alpha m}$, as seen from Eq. (8)) [41]. According to the values of ε_r, τ_ε, and α_L, the value of $\tau_{\alpha m}$ is 28.5 ppm/°C, indicating that ion polarizability of $Ca_3ZnAl_4O_{10}$ ceramic is increasing with rising temperature in the range of 25–85 °C. This result can give a good indication of rattling effect is acceptable to explain the structure-activity relationship of $Ca_3ZnAl_4O_{10}$ ceramics. The rattling effect means a weakening of the bond strength as well as the bond valence, which would correspond to an increase in ion polarizability and a decrease in energy for recovering the deformation of polyhedra. As a result, the stronger rattling effect in the series of $Ca_3ZnAl_4O_{10}$ contributes to the large $\Delta\varepsilon_r$ and the smaller $|\tau_f|$value. Recently, similar phenomena caused by rattling effect have been uncovered in $AEuV_2O_8$ (A = Bi, La) [42] and AGe_4O_9 (A = Ba, Sr) [43].

$$\tau_\varepsilon = \frac{1}{\varepsilon}\left(\frac{\partial\varepsilon}{\partial T}\right) = \frac{(\varepsilon-1)(\varepsilon+2)}{3\varepsilon}\left(\frac{1}{\alpha_m}\frac{d\alpha_m\,[T,V(T)]}{dT} - 3\alpha_L\right) \tag{7}$$

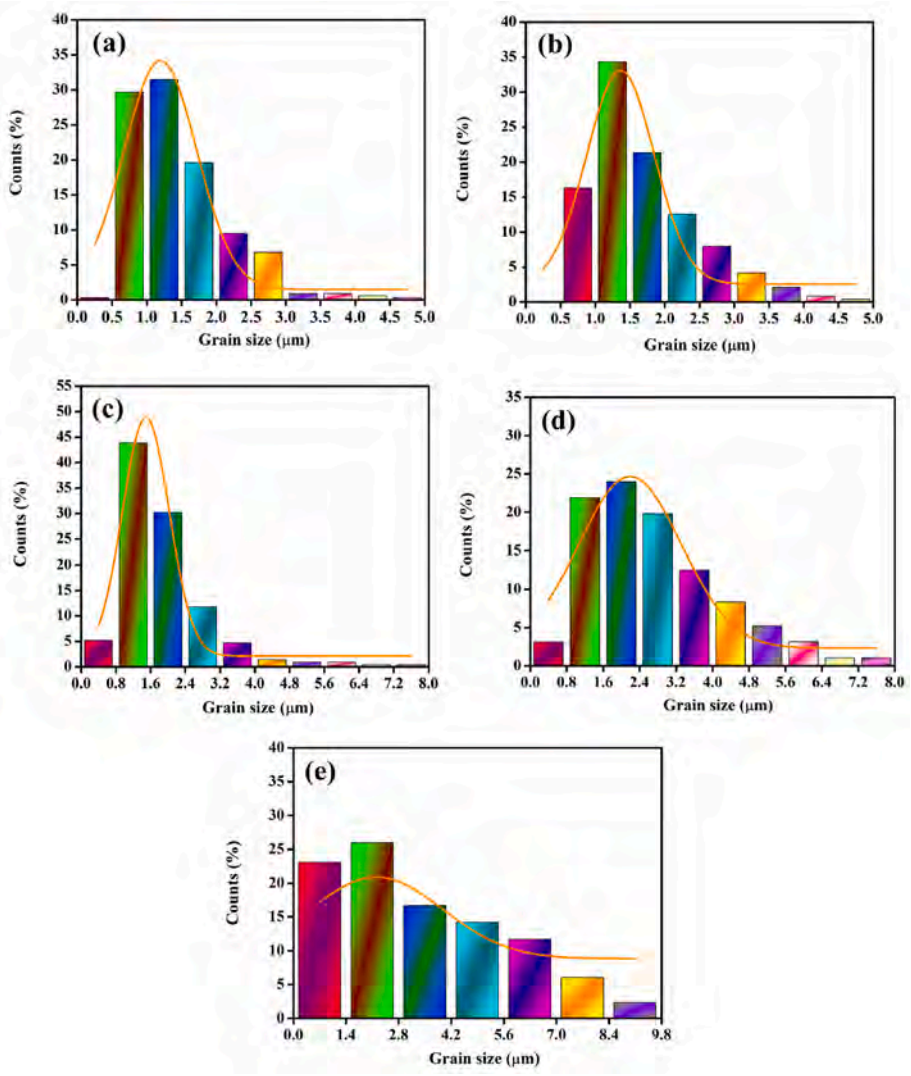

Fig. 4. The particle size distribution and average grain size of $Ca_3ZnAl_4O_{10}$ ceramics sintered at (a) 1250 °C, (b) 1270 °C, (c) 1290 °C, (d) 1310 °C, (e) 1330 °C, respectively.

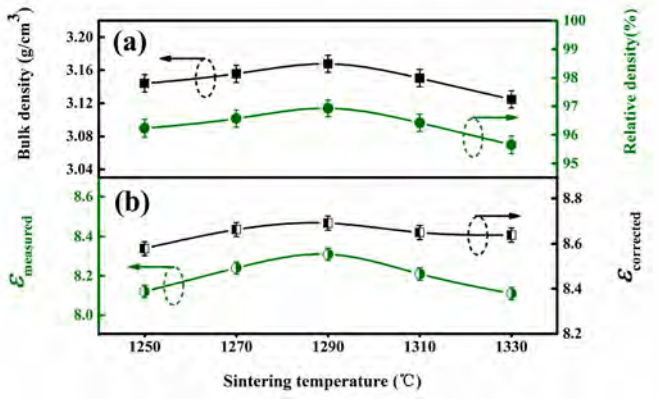

Fig. 5. The bulk density, relative density, relative permittivity, and pore-corrected permittivity of $Ca_3ZnAl_4O_{10}$ ceramics sintered at 1250–1330 °C for 6 h.

Table 3
The measured permittivity ε_r, pore-corrected permittivity ε_{corr}, theoretical permittivity ε_{theo}, and $\Delta\varepsilon_r$ of $Ca_3ZnAl_4O_{10}$ ceramics at different sintering temperatures.

S.T. (°C)	ε_r	ε_{corr}	ε_{theo}	$\Delta\varepsilon_r$ (%)
1250	8.12	8.579	6.152	39.45
1270	8.24	8.664	6.154	40.79
1290	8.31	8.693	6.155	41.23
1310	8.21	8.651	6.153	40.60
1330	8.11	8.639	6.150	40.47

$$\tau_{\alpha m} = \frac{1}{\alpha_m}\frac{d\alpha_m[T,V(T)]}{dT} \tag{8}$$

Usually, the $Q \times f$ value of the microwave ceramic relies on the two aspects of extrinsic factors and intrinsic factors. The extrinsic factors are mainly divided into the secondary phases, bulk density, porosity, and grain morphology, which can be investigated by the XRD, densimeter and SEM. The XRD patterns and Rietveld refinement results in this work show that the sintered ceramics are single-phase materials, thus the effect of secondary phase could be neglected. Therefore, densification and grain morphology are the main extrinsic loss to the $Ca_3ZnAl_4O_{10}$ ceramics. The trend of $Q \times f$ values as the sintering temperatures increased

Table 4
Bond length and bond valence of $Ca_3ZnAl_4O_{10}$ ceramic sintered at 1290 °C.

Bond type Bond length (Å)								BV (v.u.)	Ideal BV (v.u.)
Ca1-O1 Ca1-O2 Ca1-O4 Ca1-O5 Ca1-O6 Ca1-O7	Ca1-O2	Ca1-O4	Ca1-O5	Ca1-O6	Ca1-O7			1.8832	2
2.2202	2.4113	2.4909	2.4901	2.3820	2.4567				
Ca3-O1	Ca3-O2	Ca3-O5	Ca3-O8	Ca3-O9	Ca3-O10			1.7742	2
2.6144	2.4421	2.5722	2.2547	2.3839	2.3607				
Ca2-O1	Ca2-O3	Ca2-O4	Ca2-O6	Ca2-O7	Ca2-O8	Ca2-O9	Ca2-O10	1.5607	2
2.3459	2.7411	2.6304	2.4763	2.8973	2.4120	2.5854	2.8584		
Al1-O2	Al1-O3	Al1-O7	Al1-O10					2.7033	3
1.7197	1.7835	1.8468	1.8496						
Al2-O1	Al2-O2	Al2-O4	Al2-O8					2.7878	3
1.7049	1.8509	1.805	1.793						
Al3-O4	Al3-O6	Al3-O8	Al3-O9					2.9205	3
1.6775	1.7649	1.9142	1.7508						
Al4-O3	Al4-O5	Al4-O6	Al4-O7					2.5199	3
1.7985	1.8414	1.8754	1.78						
Zn-O3	Zn-O5	Zn-O9	Zn-O10					3.0115	2
1.9126	1.7745	1.7745	1.7915						

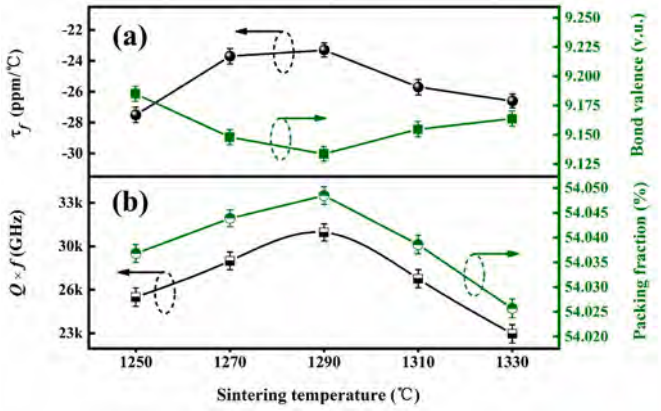

Fig. 6. (a) The relationship between sum of cation bond valence and τ_f values of $Ca_3ZnAl_4O_{10}$ ceramics sintered at different temperatures; (b) The relationship between packing fraction and $Q\times f$ values of samples sintered at various temperatures.

were similar to that of the relative density, which might be due to the elimination of porosity inside the ceramic during densification. Besides, the small grains are usually accompanied by more boundaries and comes about the lattice mismatch with higher dielectric loss consequently. Hence, the promotion of $Q\times f$ value was caused by the combined factors of the densification and normal grain growth in ceramic. When the sintering temperature rose from 1290 °C to 1330 °C, the relative density exhibited a downward trend as well as the $Q\times f$ value decreased from 30,750 GHz to 23,060 GHz. The reason for this phenomenon could be related to the high sintering temperature, which would lead to the abnormal grain growth with blurred grain boundaries and destroy the uniformity in microstructure, and thereupon increase the dielectric loss of the ceramics [44]. The packing fraction, lattice vibrations, bond strength, lattice energy, and other parameters related to the crystal structure are common intrinsic factors, specifically, a higher packing fraction (*P.f.*) stands for a smaller space for the lattice vibration and thus avoiding the higher dielectric loss [45–47]. The packing fraction of $Ca_3ZnAl_4O_{10}$ ceramics is evaluated using following equation:

$$\text{Packing fraction } f\ (\%) = \frac{volume\ of\ the\ atoms\ in\ the\ cell}{volume\ of\ unit\ cell} \times Z$$

$$= \frac{4\pi/3\times\left(2r_{Ca1(3)}^3+r_{Ca2}^3+r_{Zn}^3+4r_{Al}^3+10r_O^3\right)}{V}\times 4 \quad (9)$$

where $r_{Ca1(3)} = 1.12$ Å; $r_{Ca2} = 1$ Å; $r_{Zn} = 0.6$ Å; $r_{Al} = 0.39$ Å; $r_O = 1.38$ Å

Table 5
Bond valence, packing fraction (*P.f.*) and microwave dielectric properties of $Ca_3ZnAl_4O_{10}$ ceramics at different sintering temperatures.

		S.T. (°C)				
		1250	1270	1290	1310	1330
[Ca1O6] octahedra	BV (v.u.)	2.0083	1.9081	1.8832	1.8546	1.8021
[Ca2O6] octahedra	BV (v.u.)	1.7094	1.7529	1.7742	1.8108	1.8618
[Ca2O8] square antiprism	BV (v.u.)	1.5521	1.5591	1.5607	1.5419	1.5492
[Al1O4] tetrahedra	BV (v.u.)	2.7278	2.6795	2.7033	2.7292	2.7077
[Al2O4] tetrahedra	BV (v.u.)	2.9819	2.9176	2.7878	2.8876	2.9687
[Al3O4] tetrahedra	BV (v.u.)	2.8541	2.8739	2.9205	2.9040	2.8806
[Al4O4] tetrahedra	BV (v.u.)	2.4059	2.4841	2.5199	2.5026	2.4371
[ZnO4] tetrahedra	BV (v.u.)	3.0317	3.0197	3.0115	3.0243	3.0343
[CaO6] octahedra	Mean BV (v.u.)	1.8589	1.8305	1.8287	1.8327	1.8319
[AlO4] tetrahedra	Mean BV (v.u.)	2.7424	2.7388	2.7329	2.7559	2.7485
Cation BV sum (v.u.)		9.1851	9.1481	9.1337	9.1548	9.1639
ε_r		8.12	8.24	8.31	8.21	8.11
$Q\times f$ (GHz)		25,840	28,590	30,750	27,240	23,060
τ_f (ppm/°C)		−27.5	−23.7	−23.3	−25.7	−26.6
P.f. (%)		54.037	54.044	54.049	54.039	54.026

are the effective radii of the ions. As plotted in Fig. 6 (b), the trend of $Q\times f$ value and packing fraction is in good agreement. However, the $Q\times f$ values of these ceramics are unsatisfactory with the maximum value of 30,750 GHz. The anharmonic vibration in a distorted polyhedra might be facilitated by the strong rattling effect thereupon deteriorates the $Q\times f$. Ion doping or substitution is a good way to improve the $Q\times f$ value of the materials in some previous work [48–50], and this idea will be applied in the performance modification of $Ca_3ZnAl_4O_{10}$ ceramics in the future. In summary, the advantages of $Ca_3ZnAl_4O_{10}$ ceramics over other Al-rich compounds in Table 1 are the markedly lower sintering temperature, the obvious smaller $|\tau_f|$value and a relatively low ε_r.

4. Conclusions

Microwave dielectric ceramics $Ca_3ZnAl_4O_{10}$ with low-ε_r were synthesized using standard solid-state method. The crystal structure, sintering behaviour, microstructure of $Ca_3ZnAl_4O_{10}$ ceramics were systematically investigated together with their effects on the properties.

The XRD pattern and Rietveld refinement indicate the $Ca_3ZnAl_4O_{10}$ formation a single orthorhombic structure phase with a *Pbc21* space group. A well-packed grains and homogeneous microstructure were observed at 1290 °C. The optimal properties were obtained with ε_r = 8.31, $Q\times f$ = 30,750 GHz and τ_f = −23.3 ppm/°C. The large positive deviations ($\Delta\varepsilon_r$ = 39.45–41.23 %) between ε_{theo} and ε_{corr} could be ascribed to the strong rattling effect. The bond valence results show that the Ca^{2+} adopted eight-coordinated behaves a more active "rattling" cation. Also, the variation in τ_f could be correlated with the rattling effect and the sum of cation bond valence. The variation in the $Q\times f$ values is congruously related to the density and the packing fraction.

Declaration of competing interest

We declare that we have no financial and personal relationships with other people or organizations that can inappropriately influence our work. There is no professional or other personal interest in any product, service or company.

Acknowledgments

This work was supported by the Natural Science Foundation of Guangxi Zhuang Autonomous Region (Nos. 2022GXNSFAA035619 and 2018GXNSFBA281093), and the high-level personnel Research Funds of Yulin Normal University (grant no. G2022ZK04).

Appendix A. Supplementary data

Supplementary data to this article can be found online at https://doi.org/10.1016/j.ceramint.2023.12.103.

References

[1] J. Bao, Y.G. Chen, Y.Y. Zhou, W.J. Guo, Y.P. Zhang, J.L. Du, H.T. Wu, Z.X. Yue, Crystal structure, chemical bond characteristics, and microwave dielectric properties of novel Sr_2CaMoO_6 ceramic at different sintering temperatures, Ceram. Int. 49 (1) (2023) 335–344.
[2] B.F. Zhao, X.Q. Chen, N.C. Chen, X.W. Xu, Y.N. Lu, J. Cheng, H. Wang, Low-temperature-sintered MgO-based microwave dielectric ceramics with ultralow loss and high thermal conductivity, J. Am. Ceram. Soc. 106 (2) (2023) 1159–1169.
[3] F.F. Wu, D. Zhou, C. Du, D.M. Xu, R.T. Li, Z.Q. Shi, M.A. Darwish, T. Zhou, H. Jantunen, Design and fabrication of a satellite communication dielectric resonator antenna with novel low loss and temperature stabilized $(Sm_{1-x}Ca_x)(Nb_{1-x}Mo_x)O_4$ (x = 0.15−0.7) microwave ceramics, Chem. Mater. 35 (1) (2023) 104–115.
[4] P. Wu, H.Y. Yang, H.C. Yang, L. Gui, Y.C. Wang, Q. Liu, E.Z. Li, Synthesis of a low-firing $BaSi_2O_5$ microwave dielectric ceramics with low dielectric constant, Ceram. Int. 48 (12) (2022) 17289–17297.
[5] S. Li, C. Li, M.M. Mao, K.X. Song, Y. Lqbal, A. Khesro, S.S. Faouri, Z.L. Lu, B. Liu, S. K. Sun, D.W. Wang, High $Q\times f$ values of Zn-Ni co-modified $LiMg_{0.9}Zn_{0.1-x}Ni_xPO_4$ microwave dielectric ceramics for 5G/6G LTCC modules, J. Eur. Ceram. Soc. 42 (13) (2022) 5684–5690.
[6] H.C. Yang, S.R. Zhang, Q.Y. Wen, Y. Yuan, E.Z. Li, Synthesis of $CaAl_{2x}B_2O_{4+3x}$: novel microwave dielectric ceramics with low permittivity and low loss, J. Eur. Ceram. Soc. 41 (4) (2021) 2596–2601.
[7] X.R. Zhang, C.Y. Liu, R. Liu, Z.T. Chai, F. Guo, G.M. Wang, J.H. Liu, F. Sun, Z. X. Zhang, Coordinating microwave dielectric and optical properties of transparent yttrium aluminum garnet ceramics by regulating spark plasma sintering parameters, Mater. Sci. Eng. B. Solid. State. Mater. Adv. Technol. 260 (2020), 114628.
[8] W.C. Lou, K.X. Song, F. Hussain, A. Khesro, J.W. Zhao, H.B. Bafrooei, T. Zhou, B. Liu, M.M. Mao, K.W. Xu, E.T. Nassaj, D. Zhou, S.J. Luo, S.K. Sun, H.X. Lin, D. W. Wang, Microwave dielectric properties of $Mg_{1.8}R_{0.2}Al_4Si_5O_{18}$ (R = Mg, Ca, Sr, Ba, Mn, Co, Ni, Cu, Zn) cordierite ceramics and their application for 5G microstrip patch antenna, J. Eur. Ceram. Soc. 42 (5) (2022) 2254–2260.
[9] Z. Xing, C.Z. Yin, Z.Z. Yu, J. Khaliq, C.C. Li, Synthesis of $LiBGeO_4$ using compositional design and its dielectric behaviors at RF and microwave frequencies, Ceram. Int. 46 (14) (2020) 22460–22465.
[10] C.J. Pei, Y. Li, J.J. Tan, G.G. Yao, Y.M. Jia, W.H. Liu, P. Liu, H.W. Zhang, Temperature stable $(1-x)NaCa_4V_5O_{17}$-$xBaV_2O_6$ microwave dielectric ceramics for ULTCC applications, Ceram. Int. 46 (17) (2020) 27579–27583.
[11] X.Q. Chen, H. Li, P.C. Zhang, G.S. Li, Microwave dielectric properties of $Co_2P_2O_7$ ceramics, Ceram. Int. 47 (2) (2021) 1980–1985.
[12] X. Zhou, Z.J. Qing, H.P. Zou, H.Y. Li, A. Liu, S.M. Duan, Y.X. Li, Raman spectra, bond characteristics, and microwave dielectric properties of $Gd_2Mo_3O_{12}$ ceramics, J. Eur. Ceram. Soc. 43 (13) (2023) 5535–5539.
[13] X.K. Lan, J. Li, J.P. Li, F. Wang, W.Z. Lu, X.C. Wang, W. Lei, Phase evolution and microwave dielectric properties of novel $LiAl_{5-x}Zn_xO_{8-0.5x}$-based ($0 \le x \le 0.5$) ceramics, J. Am. Ceram. Soc. 103 (2) (2020) 1105–1112.
[14] Y. Wu, C.C. Hu, B. Liu, Y.H. Huang, K.X. Song, Crystal structure, vibrational spectroscopy, and microwave dielectric properties of $CaAl_4O_7$ ceramics with low permittivity, J. Mater. Sci. Mater. Electron. 31 (2020) 4520–4526.
[15] K.M. Manu, T. Joseph, M.T. Sebastian, Temperature compensated $Sr_2Al_2SiO_7$ ceramic for microwave applications, Mater. Chem. Phys. 133 (1) (2012) 21–23.
[16] K. Du, T.L. Wen, M.D. Zhou, Z.Y. Liu, C.Z. Yin, W. Zhu, C. Zhou, B.H. Zhang, S. X. Wang, W. Lei, Optimized phase compositions and microwave dielectric properties of low loss $Ca_2Sn_2Al_2O_9$-based ceramics by M^{4+} substitution, J. Am. Ceram. Soc. 106 (5) (2023) 2941–2952.
[17] I.J. Induja, M.T. Sebastian, Microwave dielectric properties of mineral sillimanite obtained by conventional and cold sintering process, J. Eur. Ceram. Soc. 37 (5) (2017) 2143–2147.
[18] W. Lei, R. Ang, X.C. Wang, W.Z. Lu, Phase evolution and near-zero shrinkage in $BaAl_2Si_2O_8$ low-permittivity microwave dielectric ceramics, Mater. Res. Bull. 50 (2014) 235–239.
[19] C. Du, H.H. Guo, D. Zhou, H.T. Chen, J. Zhang, W.F. Liu, J.Z. Su, H.W. Liu, Dielectric resonator antennas based on high quality factor $MgAl_2O_4$ transparent dielectric ceramics, J. Mater. Chem. C 8 (2020) 14880–14885.
[20] B. Liu, C.C. Hu, Y.H. Huang, H.B. Bafrooei, K.X. Song, Crystal structure, infrared reflectivity spectra and microwave dielectric properties of $CaAl_2O_4$ ceramics with low permittivity, J. Alloys Compd. 791 (2019) 1033–1037.
[21] K. Du, C.Z. Yin, W. Zhu, C. Zhou, B.H. Zhang, T.T. Wang, S.X. Wang, W. Lei, Phase compositions and crystal structure of Sn-deficient $Ca_2Sn_2Al_2O_9$ microwave dielectric ceramics with high $Q\times f$ values, Ceram. Int. 49 (1) (2023) 202–209.
[22] K.P. Surendran, M.T. Sebastian, M.V. Manjusha, J. Philip, A low loss, dielectric substrate in $ZnAl_2O_4$–TiO_2 system for microelectronic applications, J. Appl. Phys. 98 (4) (2005), 044101.
[23] X.K. Lan, J. Li, Z.Y. Zou, G.F. Fan, W.Z. Lu, W. Lei, Lattice structure analysis and optimised microwave dielectric properties of $LiAl_{1-x}(Zn_{0.5}Si_{0.5})_xO_2$ solid solutions, J. Eur. Ceram. Soc. 39 (7) (2019) 2360–2364.
[24] V.D. Barbanyagre, T.I. Timoshenko, A.M. Ilyinets, V.M. Shamshurov, Calcium aluminozincates of $Ca_xAl_yZn_kO_n$ composition, Powder Diffr. 12 (1) (1997) 22–26.
[25] M.M. Shang, S. Huang, J. Lin, Multicolor emissions and photoluminescence properties for $Ca_3Al_4ZnO_{10}$: Ce^{3+}/Eu^{3+}/Tb^{3+}/Mn^{2+} phosphors, J. Lumin. 204 (2018) 493–498.
[26] L.L. Sun, B. Devakumar, J. Liang, S.Y. Wang, Q. Sun, X.Y. Huang, Simultaneously enhanced far-red luminescence and thermal stability in $Ca_3Al_4ZnO_{10}$:Mn^{4+} phosphor via Mg^{2+} doping for plant growth lighting, J. Alloys Compd. 785 (2019) 312–319.
[27] V. Kahlenberg, C. Hejny, H. Krüger, Thermal expansion and compressibility of $Ca_3Al_4ZnO_{10}$ – an unusual tetrahedral framework structure, J. Solid State Chem. 276 (2019) 319–330.
[28] C. Zhang, R.Z. Zou, J. Zhang, Y. Wang, Structure-dependent microwave dielectric properties and middle temperature sintering of forsterite $(Mg_{1-x}Ni_x)_2SiO_4$ ceramics, J. Am. Ceram. Soc. 98 (3) (2015) 702–710.
[29] J. Bao, J.L. Du, L.T. Liu, H.T. Wu, Y.Y. Zhou, Z.X. Yue, A new type of microwave dielectric ceramic based on K_2O–SrO–P_2O_5 composition with high quality factor and low sintering temperature, Ceram. Int. 48 (1) (2022) 784–794.
[30] S.C. Liu, X.Q. Chen, P.C. Zhang, Q.Z. Wen, L.Z. Ma, H. Li, A novel microwave dielectric ceramic $La_5Sn_4O_{15}$ with medium-permittivity and low loss, Ceram. Int. 49 (1) (2023) 95–100.
[31] A.J. Bosman, E.E. Havinga, Temperature dependence of dielectric constants of cubic ionic compounds, Phys. Rev. 129 (1963) 1593–1600.
[32] E.E. Havinga, The temperature dependence of dielectric constant, J. Phys. Chem. Solid. 18 (1961) 253–255.
[33] R.D. Shannon, Dielectric polarizabilities of ions in oxides and fluorides, J. Appl. Phys. 73 (1993) 348–366.
[34] J.D. Dunitz, L.E. Orgel, Stereochemistry of ionic solids, Adv. Inorg. Chem. Radiochem. 2 (1960) 45–52.
[35] C. L, J.L. Hou, Z.J. Ye, R. Muhammad, A.H. Li, M.T. Ma, G.F. Wu, K.X. Song, T. Zhou, M.M. Mao, B. Liu, H.B. Bafrooei, E.T. Nassaj, S.J. Luo, F. Shi, S.K. Sun, D. W. Wang, Lattice occupying sites and microwave dielectric properties of Mg^{2+}–Si^{4+} co-doped $Mg_xY_{3-x}Al_{5-x}Si_xO_{12}$ garnet typed ceramics, J. Mater. Sci. Mater. Electron. 33 (2022) 2116–2124.
[36] Y.M. Dai, J.W. Chen, Y. Tang, H.C. Xiang, J. Li, L. Fang, Relationship between bond characteristics and microwave dielectric properties of $REVO_4$ (RE = Yb, Ho) ceramics, Ceram. Int. 49 (1) (2023) 875–881.
[37] N.E. Brese, M. O'Keeffe, Bond-valence parameters for solids, Acta Crystallogr. B: Struct. Sci. Crystallogr. Cryst. Chem. 47 (1991) 192–197.
[38] J.C. Qin, Z.F. Liu, M.S. Ma, F. Liu, Z.M. Qi, Y.X. Li, Structure and microwave dielectric properties of gillespite-type $ACuSi_4O_{10}$ (A = Ca, Sr, Ba) ceramics and quantitative prediction of the $Q\times f$ value via machine learning, ACS Appl. Mater. Interfaces 13 (2021) 17817–17826.
[39] X. Zhang, C. Liu, L. Shi, W.H. Xu, H.Y. Zhang, R. Zeng, H.W. Zhang, Ti^{4+} modified $MgZrNb_2O_8$ microwave dielectric ceramics with an ultra-high quality factor, J. Am. Ceram. Soc. 104 (11) (2021) 6054–6063.
[40] Y. Yang, Y.F. Zhai, H.C. Xiang, J. Li, Y. Tang, L. Fang, Rattling effects on microwave dielectric properties of $Ca_3TiBGe_3O_{12}$ (B = Mg, Zn) garnets, J. Eur. Ceram. Soc. 42 (11) (2022) 4566–4572.
[41] L.X. Li, Y.T. Li, J.L. Qiao, M.K. Du, Developing high-$Q\times f$ value $MgNb_{2-x}Ta_xO_6$ ($0 \le x \le 0.8$) columbite ceramics and clarifying the impact mechanism of dielectric loss: crystal structure, Raman vibrations, microstructure, lattice defects, chemical bond

characteristics, structural parameters, and microwave dielectric properties in-depth studies, J. Mater. Sci. Technol. 146 (2023) 186–199.
[42] X.W. Hu, J.W. Chen, J. Li, H.C. Xiang, Y. Tang, L. Fang, Contrasting microwave dielectric properties of zircon-structured $AEuV_2O_8$ (A = Bi, La) ceramics, J. Eur. Ceram. Soc. 42 (16) (2022) 7461–7467.
[43] F.H. Li, Y. Tang, J. Li, W.S. Fang, L.Y. Ao, Y. Wang, X.G. Zhao, L. Fang, Effect of A-site cation on crystal structure and microwave dielectric properties of AGe_4O_9 (A = Ba, Sr) ceramics, J. Eur. Ceram. Soc. 41 (7) (2021) 4153–4159.
[44] B. Li, L. Qiu, H.S. Leng, Effect of Mg^{2+} substitution on the crystal structure and microwave dielectric properties of $Ca_5Mn_4(VO_4)_6$ ceramics, Mater. Res. Bull. 118 (2019), 110510.
[45] F.Y. Huang, H. Su, Q. Zhang, Y.X. Li, Q.H. Lu, X.L. Tang, Crystal structure and performance modification of a novel triclinic $CaMgP_2O_7$ microwave dielectric ceramic with low sintering temperature, J. Eur. Ceram. Soc. 43 (8) (2023) 3338–3343.
[46] M. Yang, H.X. Zou, H.M. Yang, Y. Zheng, X.Y. Xu, M. Chen, H.F. Liang, X. Zhang, Phase composition and microwave dielectric properties of $NaSrB_{5+5x}O_{9+7.5x}$ composite ceramics, J. Eur. Ceram. Soc. 43 (5) (2023) 1964–1971.
[47] S.M. Zhai, P. Liu, G.G. Yao, S.S. Zhang, J.X. You, Novel series of high-Q oxyfluoride microwave dielectric ceramics for LTCC applications, J. Alloys Compd. 899 (2022), 163145.
[48] H.R. Tian, J.J. Zheng, L.T. Liu, H.T. Wu, H. Kimura, Y.Z. Lu, Z.X. Yue, Structure characteristics and microwave dielectric properties of $Pr_2(Zr_{1-x}Ti_x)_3(MoO_4)_9$ solid solution ceramic with a stable temperature coefficient, J. Mater. Sci. Technol. 116 (2022) 121–129.
[49] X. Zhou, L.T. Liu, J.J. Sun, N.K. Zhang, H.Z. Sun, H.T. Wu, W.H. Tao, Effects of $(Mg_{1/3}Sb_{2/3})^{4+}$ substitution on the structure and microwave dielectric properties of $Ce_2Zr_3(MoO_4)_9$ ceramics, J. Adv. Ceram. 10 (2021) 778–789.
[50] J. Bao, Y.P. Zhang, H. Kimura, H.T. Wu, Z.X. Yue, Crystal structure, chemical bond characteristics, infrared reflection spectrum, and microwave dielectric properties of $Nd_2(Zr_{1-x}Ti_x)_3(MoO_4)_9$ ceramics, J. Adv. Ceram. 12 (1) (2023) 82–92.